Atmos. Meas. Tech., 7, 199–214, 2014
www.atmos-meas-tech.net/7/199/2014/
doi:10.5194/amt-7-199-2014

Atmospheric Measurement Techniques
Open Access

An instrument for measurements of BrO with LED-based Cavity-Enhanced Differential Optical Absorption Spectroscopy

D. J. Hoch[1], J. Buxmann[1,2,*], H. Sihler[1,3], D. Pöhler[1], C. Zetzsch[2], and U. Platt[1]

[1]Institute of Environmental Physics, University of Heidelberg, Heidelberg, Germany
[2]Atmospheric Chemistry Research Laboratory, University of Bayreuth, Bayreuth, Germany
[3]Max-Planck-Institute for Chemistry, Mainz, Germany
[*]now at: Met Office, Exeter, UK

Correspondence to: U. Platt (ulrich.platt@iup.uni-heidelberg.de)

Received: 16 May 2013 – Published in Atmos. Meas. Tech. Discuss.: 2 July 2013
Revised: 29 November 2013 – Accepted: 3 December 2013 – Published: 27 January 2014

Abstract. The chemistry of the troposphere and specifically the global tropospheric ozone budget is affected by reactive halogen species such as bromine monoxide (BrO) or chlorine monoxide (ClO). Especially BrO plays an important role in the processes of ozone destruction, disturbance of NO_x and HO_x chemistry, oxidation of dimethyl sulfide (DMS), and the deposition of elementary mercury. In the troposphere BrO has been detected in polar regions, at salt lakes, in volcanic plumes, and in the marine boundary layer. For a better understanding of these processes, field measurements as well as reaction chamber studies are performed. In both cases instruments with high spatial resolution and high sensitivity are necessary. A Cavity-Enhanced Differential Optical Absorption Spectroscopy (CE-DOAS) instrument with an open path measurement cell was designed and applied. For the first time, a CE-DOAS instrument is presented using an UV LED in the 325–365 nm wavelength range. In laboratory studies, BrO as well as HONO, HCHO, O_3, and O_4 could be reliably determined at detection limits of 20 ppt for BrO, 9.1 ppb for HCHO, 970 ppt for HONO, and 91 ppb for O_3, for five minutes integration time. The best detection limits were achieved for BrO (11 ppt), HCHO (5.1 ppb), HONO (490 ppt), and O_3 (59 ppb) for integration times of 81 minutes or less. Comparison with established White system (WS) DOAS and O_3 monitor measurements demonstrate the reliability of the instrument.

1 Introduction

Besides their well known effects on stratospheric ozone, reactive halogen species (RHS) are responsible for a series of phenomena in various compartments of the troposphere that includes volcanic plumes, coastal areas, salt lakes, and the polar boundary layer. For instance, RHS, and especially bromine, are of scientific interest because they are mainly responsible for ozone depletion in the arctic boundary layer during polar spring. This phenomenon was first observed by Bottenheim et al. (1986), and several other studies followed that established a link between O_3 depletion and RHS (e.g., Barrie et al., 1988, 1994; Hausmann and Platt, 1994; Bottenheim et al., 1990; Sturges et al., 1993; Platt and Lehrer, 1996; Kreher et al., 1997; Tuckermann et al., 1997). The halogen catalyzed ozone depletion events occur only during polar sunrise. The release mechanism for reactive bromine is described by the "bromine explosion" mechanism (Platt and Lehrer, 1996). The phenomenon is still not completely understood and is the subject of current research (Saiz-Lopez et al., 2007; Pöhler et al., 2010; Friess et al., 2011).

Also outside polar regions RHS strongly affect the ozone budget and the oxidation capacity of the atmosphere. Bromine monoxide (BrO) was detected in the mid-latitude marine boundary layer at different locations (Leser et al., 2003; Saiz-Lopez et al., 2004; Read et al., 2008; Mahajan et al., 2010). At salt lakes high mixing ratios of BrO could be detected, up to 20 ppt at the Salar de Uyuni, Bolivia, (Hönninger et al., 2004) and up to 220 ppt at the Dead Sea

(Hebestreit et al., 1999; Matveev et al., 2001; Tas et al., 2008). Most of these observations were performed with long-path or multi-axial differential optical absorption spectroscopy (LP-DOAS or MAX-DOAS, respectively) measurement techniques averaging the concentration over several kilometers. For a better understanding of the involved processes, field measurements with high spatial resolution are essential. Cavity-enhanced (CE) DOAS offers the opportunity of mobile in situ measurements of RHS without the risk of inlet and wall losses. In addition, RHS release, transformation, and loss processes can be studied in reaction chambers (e.g., Buxmann et al., 2012; Ofner et al., 2012). For these studies, compact yet highly sensitive instruments for RHS measurements are also required.

O'Keefe and Deacon (1988) started to use optical cavities with highly reflective mirrors to observe absorbers by applying cavity ring-down spectroscopy (CRDS). With this approach, the decay of light intensity leaking from the resonator after switching off the pump light source is measured. Since then the technique has been continuously refined (Zalicki and Zare, 1995; Paldus et al., 2000; Ball et al., 2001; Fawcett et al., 2002; Simpson, 2003; Ball and Jones, 2003; Schuster et al., 2009). A limitation of most CRDS instruments is that any extinction (absorptions or scattering) beside that of the investigated trace gas at the applied wavelength leads to interferences and must be avoided. Thus, measurements at spectral ranges where several molecules absorb cannot be used (e.g., the UV spectral range due to O_3 and NO_2 absorptions). Additionally this requires the removal of aerosols and thus typically demands closed resonators with aerosol inlet filters. Moreover, this approach introduces the risk of trace gas loss as well as possible chemical reactions on the inlet and filter (e.g., conversion of HOBr to Br_2, Neuman et al., 2010; or BrO self-reaction, Liao et al., 2011). A second approach, the so-called cavity-enhanced absorption spectroscopy (CEAS), was developed, which relies on measuring the transmittance of the resonator by recording the leak-out intensity (Engeln et al., 1998; Peeters et al., 2000). In contrast to CRDS, the CEAS approach uses a continuous wave (CW) source of radiation. Based on CEAS (e.g., Fiedler et al., 2003; Langridge et al., 2006; Venables et al., 2006; Orphal and Ruth, 2008; Vaughan et al., 2008; Washenfelder et al., 2008; Langridge et al., 2008; Varma et al., 2009; Chen and Venables, 2011; Chen et al., 2011), Kahan et al. (2012) applied the broadband (BB) CEAS using broadband light sources (rather than a single wavelength as in the traditional CRDS or CEAS approaches). Ball et al. (2004) combined BBCEAS for the data evaluation with the established DOAS technique (Platt and Stutz, 2008), creating the CE-DOAS. With this technique, different trace gases can be detected simultaneously and at high spatial resolution (Ball et al., 2004; Gherman et al., 2008; Platt et al., 2009; Meinen et al., 2010; Thalman and Volkamer, 2010). We note that the BBCEAS retrieval algorithm published by Fiedler et al. (2003) relies – like DOAS – on the characteristic narrow band absorption features of the molecules for their quantification and is thus in principle equivalent to DOAS. The theoretical description of CE-DOAS can be found in Platt et al. (2009). To date, to our knowledge, only two cavity-based measurement systems to detect BrO in the UV wavelength range exist (Chen and Venables, 2011; Grilli et al., 2012), and neither system applies the DOAS technique. Both of them use a heavy and highly power consuming light source (e.g., tunable laser and xenon arc lamp). This means that there is a lack of in situ instruments allowing mobile measurements of BrO radicals in the field without requiring laboratory infrastructure.

The mode-locked frequency-doubled cavity-enhanced spectrometer described by Grilli et al. (2012) has a 7 m Teflon inlet tube. Although the instrument provides BrO detection with remarkable good detection limits of 1.7 ppt at a time resolution of 30 s, there is a possible effect of inlet losses (Neuman et al., 2010; Liao et al., 2012; Buys et al., 2013). The authors state undetectable BrO losses within the relatively large concentration fluctuations of up to ± 12 ppt in an artificial air sample. This result requires further validation.

Besides cavity instruments, chemical ionization mass spectrometers (CIMS) are capable of indirect BrO detection, but complex sample preparation and calibration is needed (e.g., Neuman et al., 2010; Liao et al., 2011). This limits the application of these instruments for field studies, where low power consumption, simple operation, and a lightweight setup is required. Additionally, loss or chemical conversion of highly reactive compounds (e.g., BrO or HOBr) on instrument and inlet surfaces occur and can even result in a complete loss of BrO, which can influence the indirect detection of BrO with CIMS instruments (Neuman et al., 2010). Nevertheless, it was demonstrated by Liao et al. (2011) that reliable BrO concentrations can be provided by an optimized and very short inlet CIMS instrument. These measurements were found to be in good agreement with a well established long-path DOAS system (Liao et al., 2011).

Our paper describes the design and development of a specific CE-DOAS instrument, which, for the first time, identifies BrO in the UV wavelength range (325–365 nm) by applying an UV LED. Compared to the xenon arc lamps applied as light sources in previous experiments, UV LEDs offer several advantages particularly important for cavity-enhanced measurements: (1) the relatively narrow emission spectrum of LEDs reduces the amount of stray light within the instrument because there is no light emitted outside the spectral range of the high mirror reflectivity. Hence, fewer spectral filters are required, the risk of systematic measurement errors is reduced and the instrument setup becomes less complex. (2) The light output of LEDs can be easily modulated. It is thus possible with the instrument presented here to monitor the effective path length by measuring the ring-down time between measurements. (3) The lifetime of LEDs is typically longer than for arc lamps. This reduces maintenance and the costs of operation are thus lowered. (4) LEDs are much easier to handle than arc lamps and do not, for instance,

require a special housing or high voltage for ignition. The power consumption is by far lower, as mentioned above, and less excess heat is produced. This is particularly useful when the light-source is applied in temperature-controlled environments like smog chambers.

Compared to instruments designed for the visible to infrared spectral range wavelength range, Rayleigh scattering and parasitic mirror losses become important in the UV and thus reduce the achievable maximum path length. Both effects are discussed in this paper. To estimate the optical path length in the cavity, the instrument applies the cavity ring-down technique (Meinen et al., 2010) and additionally the measurements of the trace gases O_4, O_3, and HONO. At the Atmospheric Chemistry Research Laboratory of the University of Bayreuth, Germany, first laboratory measurements were successfully performed and the detection limits for different trace gases were determined. Also, we compare the CE-DOAS results with an established White system (WS) DOAS for detection of O_3, HCHO, NO_2, HONO, O_4, OClO and SO_2 and a chemiluminescence O_3 monitor.

2 Method: cavity-enhanced differential absorption spectroscopy (CE-DOAS)

The basic idea of the CE-DOAS technique is to introduce incoherent broadband radiation with the intensity I_L into an optical resonator (see Fig. 1), consisting of two mirrors with reflectivity R (for simplicity we assume both mirrors to have the same reflectivity; if the mirrors have different reflectivities R_1, R_2, an averaged reflectivity $R = \sqrt{R_1 R_2}$ is used). The distance between the mirrors is d_0 (see Fig. 1). Initially only the fraction $\rho = 1 - R$ of the radiation I_L enters the resonator. Here for simplicity I_L means only the fraction of the radiation from the LED which can be imaged into the resonator. (It is obvious that not all radiation emitted by the LED is passing through the lens and also passes the aperture defined by mirror M_2.) Once inside the resonator, the radiation is reflected on average $1/(1-R)$ times (neglecting other losses). Finally, in the absence of any extinction in the resonator, half of the radiation leaves the resonator through each mirror. The radiation (intensity I_{tot}) leaving the cavity through the mirror opposite the light source (see Fig. 1) is available for further analysis, as described below.

The DOAS techniques derive the trace gas concentration by the use of the optical density $D(\lambda)$, which requires the measurement of the intensities without ($I_0(\lambda)$) and with ($I(\lambda)$) trace gas absorption (Platt and Stutz, 2008). In a CE-DOAS setup the optical density $D_{\mathrm{CE}}(\lambda)$ is determined from intensity measurements with absorber free filled (e.g., synthetic air) resonator I_{tot0} and with sample air filled resonator I_{tot} (Platt et al., 2009):

$$D_{\mathrm{CE}}(\lambda) = \ln\left(\frac{I_{\mathrm{tot0}}(\lambda)}{I_{\mathrm{tot}}(\lambda)}\right) = \ln\left(\frac{\int_0^\infty I_{\mathrm{in0}}(\lambda, n)\,\mathrm{d}n}{\int_0^\infty I_{\mathrm{in}}(\lambda, n)\,\mathrm{d}n}\right), \qquad (1)$$

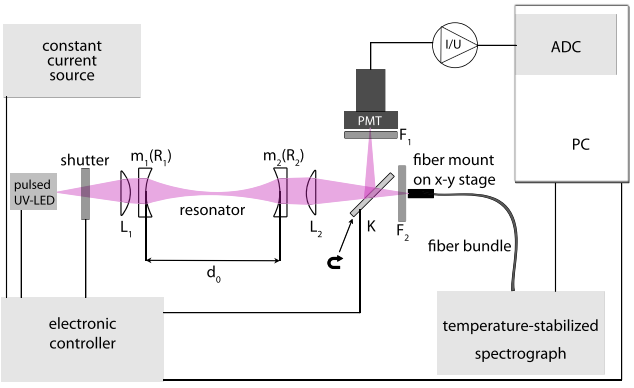

Fig. 1. Schematic diagram of the CE-DOAS instrument. The radiation output of a pulsed UV LED is imaged by lens L_1 into the resonator consisting of two highly reflective dielectric mirrors M_1 and M_2. The light which leaves the resonator through M_2 is focused by the lens L_2 to a fiber bundle attached to an x–y stage. This fiber bundle transmits the light to a temperature stabilized spectrograph (Ocean Optics QE 65000). Alternatively, the movable mirror "K" can redirect the light to a photomultiplier (PMT) to optionally record a ring-down signal and thus check the path length of the resonator. F_1 and F_2 are band-pass filters (Schott UG11). F_1 protects the PMT and F_2 the fibers from scattered light and LED radiation outside of the reflectivity range of the mirrors. The shutter is used to perform background measurements. The electronic controller receives a constant current and creates the pulses for the UV LED. It also controls the shutter and the mirror K.

where $I_{\mathrm{in0}}(n)$ is the intensity after n passes through the cavity in the pure air filled cavity (without any absorbers) and $I_{\mathrm{in}}(n)$ is the intensity after n passes through the cavity also including absorptions. n is the number of traverses of the photons through the cavity. However, according to Platt et al. (2009), for strong absorptions this is not equal to the optical density $D(\lambda)$ used in traditional DOAS applications if using the average light path from Sect. 2.1. Thus, the corrections described in Sect. 2.3 have to be applied.

2.1 Determination of the average path length

A theoretical description of the average path length can be found in Platt et al. (2009). In practice, this average path length $\overline{L}_0(\lambda)$ can be determined from the known Rayleigh scattering of two different gases, e.g., helium and dry zero air (Washenfelder et al., 2008), from a CRD decay time measurement (Meinen et al., 2010) or from the differential absorption of a trace gas of known concentration. In this work $\overline{L}_0(\lambda)$ was determined from the absorption bands of O_4 at 343.5 and 360.4 nm, making use of the known O_2 concentration (Ball et al., 2004). The following subsections describe how this average path length has to be corrected.

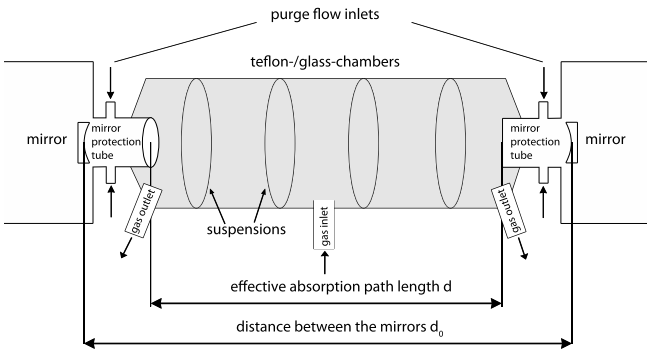

Fig. 2. Setup for the measurements at the Atmospheric Chemistry Research Laboratory, University of Bayreuth, Germany. One of three air-tight chambers made of either Teflon or glass is placed between the two mirrors. Because this chamber can be filled via the gas inlet with different trace gases, a purge flow of nitrogen in front of the mirrors avoids aerosols from the sample air to contaminate the mirrors. The distance between the mirrors is d_0. The effective absorption path length is d because the sample gas only fills the volume between the ends of the mirror protection tubes between the purge gas outlets.

2.2 Correction of the base path length

The length of the absorption medium in the resonator d is not necessarily equal to the distance between the mirrors d_0 (see Fig. 2), since at either end of the resonator usually a few centimeters of the path are not filled with sample air due to a purge flow close to the mirrors. In this case, the effective light path has to be corrected by the geometric factor d/d_0:

$$\overline{L}(\lambda) = \overline{L}_0(\lambda)\,\frac{d}{d_0}. \quad (2)$$

For measurements of a small sample volume (small chamber), the dilution of the air due to the purge flow has also been taken into account.

2.3 Correction for light path reduction due to extinction in the cavity

Platt et al. (2009) described in detail how the light path is reduced by extinction in the resonator. Here two ways to correct this effect presented by Platt et al. (2009) are applied. A more detailed explanation of method 1 is described by Horbanski (2010) and Horbanski et al. (2014). For both ways the optical density D_{CE} and the average path length $\overline{L}(\lambda)$ needs to be known.

1. Correction of the trace gas absorption cross section σ to σ_{eff}:

$$\sigma_{\mathrm{eff}}(\lambda) = \sigma(\lambda) \times \frac{\overline{L}_{\mathrm{eff}}(\lambda)}{\overline{L}(\lambda)} = \sigma(\lambda) \times \frac{D_{\mathrm{CE}}}{e^{D_{\mathrm{CE}}} - 1}. \quad (3)$$

This σ_{eff} is used by a DOAS-fit to obtain a corrected column density. From this column density the correct concentration is determined by dividing with $\overline{L}(\lambda)$. As the absolute optical density D_{CE} is difficult to measure precisely, this method is used iteratively, where the optical density D_i of the ith iteration is calculated. During the first iteration a DOAS fit determines an optical density D_0 and σ_0 is corrected to σ_1. In the next iteration step σ_1 determines a D_1 and σ_0 is corrected to σ_2, etc.:

ith iteration:

$$\sigma_i \rightarrow (\mathrm{cL})_i \rightarrow (\mathrm{cL})_i \times \sigma_i = D_i \rightarrow \sigma_0 \times \frac{D_i}{e^{D_i} - 1} = \sigma_{i+1}. \quad (4)$$

We applied this correction in four iteration steps for measurements with only one trace gas and without aerosols. The same method can also be applied if several absorbers are present by extending Eq. (4). This method has the important advantage that it does not rely on the absolute optical density D_{CE} and thus intensity I_{tot} and is thus not sensitive to any possible intensity changes of, e.g., the LED between reference and sample measurement.

2. Method 1 with Eq. (3) becomes very complex when using more than one absorber and is not applicable if aerosols are present. In this case, a second method is useful in order to correct the optical density before the fit and convert it to D_{eff}, which is equal to an absorption where the light path is not reduced:

$$D_{\mathrm{eff}} = e^{D_{\mathrm{CE}}} - 1 = \frac{I_{0\mathrm{tot}}}{I_{\mathrm{tot}}} - 1. \quad (5)$$

In this work, the second method applying Eq. (5) is used whenever there is more than one absorber. It needs to be considered that for this correction the intensities $I_{0\mathrm{tot}}$ and I_{tot} have to be successively measured. This requires an absolutely stable optical resonator and light source intensity, similar to the requirements of the BBCEAS approach.

2.4 Correction of the wavelength dependence of the average light path

As described in Sect. 2.1, the average light path $\overline{L}(\lambda)$ is also dependent on λ because $R(\lambda)$ is dependent on λ. As described by Venables et al. (2006), it is possible to use differential absorption structures for the determination of the wavelength dependence of the mirror reflectivity and therefore for the calibration of the path length. This method requires an absorber of known concentration, which has several distinct absorption bands in the wavelength range of interest. However, the relative shape of the mirror reflectivity curve can be determined from any absorber having several absorption bands within the region of high mirror reflectivity. In the present study, we used O_3 and HONO to estimate the shape of the reflectivity curve. Since the concentration

of these gases was unknown, the absorption bands of O_4 at 343.5 nm and 360.4 nm were additionally used to derive the absolute reflectivity curve of the mirrors.

3 Experimental

3.1 Instrument

Figure 1 shows a schematic diagram of the CE-DOAS instrument (more details can be found in Hoch, 2010). The radiation of a pulsed UV LED is imaged by lens L_1 into the resonator, consisting of two highly reflective dielectric mirrors M_1 and M_2 (focal length = 1 m). The radiation, which leaves the resonator through M_2, is focused by the lens L_2 into a fiber bundle which can be adjusted by a x–y translation stage. This fiber bundle transmits the light to a temperature-stabilized spectrograph (Sect. 3.1.3). The movable mirror "K" can redirect the light to a photomultiplier (PMT) to record a ring-down signal and thus check the quality of the resonator. F_1 and F_2 are band-pass filters (for details see Sect. 3.1.2). F_1 protects the PMT and F_2 shields the fibers from scattered light and LED light outside of the reflectivity range of the mirrors. The shutter is used to perform background measurements without radiation of the UV LED. The electronic controller receives a constant current and creates the pulses for the UV LED. It also controls the shutter and the mirror "K".

3.1.1 LED radiation source

The wavelength range (325 to 365 nm) of the LED UVTOP340 from Sensor Electronic Technology was chosen to optimize the sensitivity to BrO while minimizing the interference due to O_3, but still being appropriate to detect O_3. In the order to minimize the known LED etalon structures, the surface-normal of the LED-chip is inclined against the optical axis of the resonator at an angle of 15° (Sihler et al., 2009). For CRD measurements the LED has to be operated in a pulsed mode. Extensive noise characterizations of the LED showed that permanent pulsing of the LED creates less spectral noise than a periodic change between pulsing and continuous operation, while the spectrum of the LED does not change. Therefore the LED is permanently pulsed with 750 µs (on) and 50 µs (off) for also recording spectra with the spectrometer. The time required for the cavity to reach optical equilibrium is approximately 3.7 µs (for mirrors of reflectivity 0.9991 and 1 m cavity length), leading to a maximum light path of approximately 1111 m. This is small relative to the 750 µs when the LED is powered.

The UVTOP340 delivers 400 µW of optical output power (SET, 2010). This figure appears incredibly small now compared to the optical output power of a 75 W xenon arc lamp as described by Kern et al. (2006). However, the relevant quantity needed to compare the optical output of different light sources is the spectral radiance integrated over the wavelength interval used to evaluate the trace gas absorption features. On the one hand, the radiance of the UVTOP340 between 325 and 365 nm calculates to $4.2 \times 10^3\ \mathrm{W m^{-2}\ sr^{-1}}$, assuming a Lambertian emission pattern, an emitter area of $0.045\ \mathrm{mm^2}$ as derived from microscopic measurements, and a Gaussian emission spectrum (340 nm peak, 15 nm FWHM). On the other hand, the emission spectrum of a xenon arc lamp (e.g., XBO 75 W/2 xenon arc lamp manufactured by OSRAM) is approximated by that of a Planckian gray body with an emissivity of 0.17 derived from the photometric properties given in Osram (2012). The radiance of the xenon arc lamp between 325 and 365 nm calculates to $1.9 \times 10^6\ \mathrm{W m^{-2}\ sr^{-1}}$. Thus, the arc lamp has a radiance in this wavelength interval that is about 450 times higher compared to the UVTOP340. However, the optical output power in the 325 to 365 nm range per electrical input power for both devices is almost equal since the UVTOP340 consumes only 180 mW.

3.1.2 Mirrors and optics

The main component of the setup is the resonator, which consists of two highly reflective mirrors (Fig. 1, M_1 and M_2). The reflectivity of the mirrors from LAYERTEC GmbH, (Mellingen, Germany) was chosen to achieve a good compromise between optical light path length and signal-to-noise ratio (Fiedler et al., 2007). The radiation of the UV LED is coupled into the resonator by lens L_1 ($F_1 = 25$ mm) to use as much of the LED output as possible. The radiation that passes mirror M_2 is focused by lens L_2 ($F_2 = 100$ mm) on a fiber coupler to match the numerical aperture (NA[1]) of the spectrometer. The fiber bundle (Loptek GmbH & Co, Berlin, Germany) consists of seven 200 µm fibers (NA of 0.22, UV solarization stabilized, 6 m long), arranged in a circular configuration on the resonators side and column configuration at the spectrometers side. The band-pass filters F_1 and F_2, both UG11 from Schott, (Mainz, Germany), have a transmission range of 270–380 nm and a thickness of 1 mm. F_1 was placed directly in front of the PMT in order to protect the device as much as possible against ambient light (e.g., if cover is opened). The reflectivity of the mirrors cannot readily be derived from the manufacturer's data: Layertec provided transmission values (T) but not reflectivities. Since $R + T + A = 1$ (A = absorption), R cannot be calculated from T unless A in the dielectric mirror is negligible, which, unfortunately, is not the case in this wavelength range. We used two sets of mirrors with different values of stated transmissivity at 340 nm: M_1: $T = 0.048$ %, M_2: $T = 0.11$ %.

[1] $\mathrm{NA} = n \sin(\alpha/2)$, n = index of refraction = 1.0 (air), α = angular aperture (maximum cone of light that can enter or exit the optical device of interest).

3.1.3 Spectrograph and detector

The fiber transmits the light into a temperature stabilized ((20.0 ° ± 0.1) C) spectrograph QE65000 from Ocean Optics (Dunedin, Florida, USA). The spectrometer has a focal length of 101 mm and is equipped with a 2400 lines mm^{-1} grating, resulting in 0.62 nm spectral resolution with the column of seven 200 µm fibers (see Sect. 3.1.2) acting as entrance slit.

The detector used in the QE65000 spectrometer is a scientific grade, back-thinned, thermo-electrically cooled (TEC), 1044×64 element CCD array (S7031-1006 from Hamamatsu Photonics (Naka-ku, Hamamatsu City, Shizuoka Pref., Japan)), temperature stabilized to −20 °C.

3.1.4 Photomultiplier (PMT) for CRD

For the ring down measurement the radiation intensity is measured by a PMT (H578-01 from Hamamatsu Photonics (Naka-ku, Hamamatsu City, Shizuoka Pref., Japan)). As current amplifier a DLPCA-100 from FEMTO Messtechnik GmbH, (Berlin, Germany) is applied. A PC oscilloscope DAQSCOPE PCI-5102 from National Instruments (Austin, Texas, USA) records the ring-down signal.

3.1.5 Data recording and cavity ring-down calibration

The program DOASIS (Kraus, 2004) is used to control the measurements and to analyze the CE-DOAS and WS DOAS spectra.

To acquire the CRD signals, a dedicated program was developed with LabVIEW from National Instruments. This program receives the ring-down signal from the PC oscilloscope, calculates the mean of a given number of measurements and fits a double exponential decay $f(t)$ (Eq. 6):

$$f(t) = A \times \left(\frac{\tau_1}{\tau_1 - \tau_2} \times e^{-\frac{t}{\tau_1}} - \frac{\tau_2}{\tau_1 - \tau_2} \times e^{-\frac{t}{\tau_2}} \right) + b \quad (6)$$

τ_1 denotes the electro-optical decay time from electronics and LED and τ_2 for the CRD decay time. A typical value for τ_1 is 100 ns and it is determined by the rise time of the pulse electronics of the LED and the rise time of the LED output itself. Also, A denotes the initial signal at $t = 0$ and b denotes any offset signal at $t = \infty$. From this fit and known τ_1, the CRD decay time can be determined and converted to an optical light path or mirrors reflectivity according to Meinen et al. (2010). However, in our case it is not possible to derive with this method the accurate absorption light path for the data evaluation, as the mirror reflectivity varies too much over the LED spectral range (see Sect. 2.4). Nevertheless, τ_2 just gives an indication of the wavelength averaged light path, which is used to monitor the contamination of the mirrors as well as the optical alignment of the resonator. This allows quick action to optimize instrument performance. In fact, during chamber studies the UV CE-DOAS system performed with excellent stability during a time period of several days without mirror cleaning and readjustment.

3.2 The measurement setups

The instrument was developed and characterized at the Institute for Environmental Physics (IUP) in Heidelberg, Germany. After the first successful measurements, it was applied for the observation of different trace gases at the Atmospheric Chemistry Research Laboratory, University of Bayreuth, Germany. For these measurements the instrument was used as it is described in Sect. 3.1 and shown in Fig. 1. Two hermetically sealed plastic boxes were placed around the optical component assemblies in order to protect the sensitive optics against dust and other extreme conditions for planned measurements in a climate chamber. Furthermore, the hermetically sealed containment guarantees a stable nitrogen purge-flow (1 L min^{-1}) of the resonator mirrors to prevent contaminations from the measurement air. Otherwise a slight overpressure in the reaction chamber could cause a flow of unfiltered air from the chamber towards the mirrors and thus cause contaminations. For the measurements described below, an air-tight chamber was placed between the two boxes containing the mirrors and associated optics (Fig. 2). This chamber could be filled through three gas inlets/outlets with different gases. Three different setups with various base-path lengths were used: one with a glass chamber (setup A) and two with Teflon chambers (setups B and C). The glass chamber setup was the first to be used because it could be built easier than Teflon, but the cavity length is much shorter. The Teflon/glass chambers A, B and C were kept in pressure equilibrium with the laboratory with the help of two open outlets, as indicated in Fig. 2. The mirror purge flow compensates for any leakage of the chamber. Table 1 shows the sizes of these three chambers and Table 2 gives an overview of the different trace gas measurement setups. With these setups, different trace gas measurements were carried out: O_3 and HONO were measured mainly in order to determine the wavelength dependency of the mirror reflectivity and the optical path length, O_4 measurements were performed in order to determine the absolute optical path length at two particular wavelengths (343.4 and 360.5 nm), and BrO and HCHO measurements were made in order to determine the detection limits for these species. Before each trace gas measurement, offset (20 000 scans and 8 ms integration time) and dark current (1 scan and 30 000 ms integration time) spectra were taken with blocked LED. If any background radiation intensity would be present, it would be included in the dark current spectrum. In the next step a CRD measurement with 1000 average determinations was performed to determine possible mirror contamination. A spectrum with 85 % of full saturation could be obtained in 9.50 s with mirror set M_1 and 3.50 s with mirror set M_2. Based on noise tests, 30 spectral scans were taken and co-added for mirror set M_1 and 50 spectral scans were taken and co-added for mirror set

Table 1. Chamber sizes and base-path lengths for setups A, B and C.

Setup (chamber type)	Cavity length (d_0) [cm]	Absorption length (d) [cm]	Volume [L]
A (glass)	107 ± 1	47 ± 1	7.5
B (Teflon)	149 ± 1	127 ± 1	40
C (Teflon)	181 ± 1	159 ± 1	50

Table 2. Measurement setups for detection of different trace gases.

Measurement	Mirror set	Setup
O_3	M_1 and M_2	A
O_3	M_2	B
O_3	M_1	C
HONO	M_1 and M_2	A
HONO	M_2	B
HONO	M_1	C
BrO	M_2	B
BrO	M_1	C
O_4	M_1 and M_2	A
O_4	M_1	C

M_2 to achieve sufficient measurement accuracy. This corresponds to a temporal resolution of 4.8 min for M_1 and 2.9 min for M_2. The measurements shown within this study were undertaken without the presence of aerosols.

3.2.1 Ozone measurements

For the O_3 measurements the setups A, B, and C were used. For setup A both mirror sets, for setup B mirror set M_2, and for setup C mirror set M_1 were used (Table 2). To determine an I_0 spectrum the chamber was filled with nitrogen and the mirrors were purged with nitrogen, too. Afterwards O_3 was produced and filled into the chamber through the gas inlet (up to 2 ppm). The gas outlets were connected to an active charcoal trap. In setup A and B the ozone was created by ionization of O_2 (purity = 99.995 %) using a corona discharge ozonizer and in setup C by passing O_2 (purity = 99.995 %) along four Pen-Ray mercury discharge lamps.

3.2.2 Nitrous acid measurements

For the nitrous acid (HONO) measurements, setup A with both mirror sets, setup B with mirror set M_2, and setup C with mirror set M_1 were used (see Table 2), similar to the setups for O_3 measurements. The generation of the nitrous acid is based on the reaction of a sodium nitrite solution $NaNO_2$ with sulfuric acid H_2SO_4 as, e.g., described by Taira and Kanda (1990):

$$H_2SO_4 + NaNO_2 \rightarrow NaHSO_4 + HONO. \quad \text{(R1)}$$

The reaction takes place in a glass vessel with a glass frit at its base. The diluted solutions of sodium nitrite and sulfuric acid are continuously pumped into a reaction vessel and the mixture is then drawn off to waste. A carrier gas, here nitrogen, is introduced into the reagent mixture through the frit and continuously purges nitrous acid vapor from the mixture. The HONO generation depends on temperature, gas flow, $NaNO_2$ concentration and fluid flow. Typical mixing ratios up to 30 ppb were accomplished.

3.2.3 Oxygen dimer measurements

In order to determine the light path in the cavity, O_4 measurements were carried out at two particular wavelengths (343.4 and 360.5 nm). For this purpose the resonator was first completely filled with nitrogen and afterwards completely (including mirror purge gas) with pure oxygen. Additionally, barometric pressure (with a mercury barometer) and temperature were measured next to the chamber (the same values assumed as in the chamber) to determine the O_2 concentration in the resonator. With the absorption of O_4 at 343.4 and 360.5 nm, the light path at these wavelengths could be determined.

3.2.4 Bromine monoxide measurements

BrO measurements were carried out using setup B with mirror set M_2 and in setup C with mirror set M_1 (see Table 2). For these measurements the mirror protection tubes were purged with nitrogen. The gas outlets are connected to a pump producing a slight underpressure. First O_3 was admitted through the gas inlet and afterwards Br_2. A fluorescent tube (Philips TL/12, 40 W, UV A and UV B) set up next (at 20 cm distance) to the chamber was switched on to photolyze Br_2. A typical concentration up to 1000 ppt BrO was measured. Evaluation and results of these measurements are described in Sect. 4.

3.2.5 Comparison of the CE-DOAS with a White system DOAS and an ozone monitor

During experiments with a simulated salt pan (Buxmann et al., 2012) at the Atmospheric Chemistry Research Laboratory, University of Bayreuth, Germany, in the low-temperature aerosol simulation chamber (LOTASC) (http://www.eurochamp.org/chambers/lotasc/), a comparison between the CE-DOAS and a DOAS WS (White, 1942, 1976; Ritz et al., 1993; Volkamer, 1996; Volkamer et al., 2002; Hak et al., 2005) as well as the CE-DOAS and a chemiluminescence (CL) ozone monitor (Bendix-UPK8002) was performed. The cylindrical chamber, made of Teflon foil (FEP 200 A, DuPont, thickness 0.05 mm) with a diameter of 1.33 m and a volume of 3500 L, has been described in detail by Siekmann (2008); Bleicher (2012); Buxmann et al. (2012). The LOTASC was kept at a pressure slightly above atmospheric pressure in order to prevent leaking of room air into the system. The dilution rate, replenishing the loss by sampling and other outlets, was of the order of $3 \times 10^{-5}\,s^{-1}$,

Table 3. Literature absorption cross sections used in the DOAS evaluation. The cross sections were corrected with a Pre-shift and linked together for the following measurements.

Trace gas	Reference	Pre-shift [nm]	Shift
BrO	Fleischmann and Burrows (2004)	0.153	free
HCHO	Meller and Moortgat (2000)	0.0018	linked to BrO
HONO	Stutz et al. (2000)	0.08221	linked to BrO
O_4	Greenblatt et al. (1990)	0.578	linked to BrO
O_3	Voigt et al. (2001)	0.206	linked to BrO
NO_2	Voigt et al. (2002)	0	linked to BrO

which corresponds to about 4 L min^{-1} zero air input, including the purge flow (1 L min^{-1}) of the CE-DOAS mirrors (compare Buxmann et al., 2012 and Buxmann, 2012). To monitor the dilution rate, several ppb of n-perfluorohexane, a chemically inert dilution standard, is added before the start of the experiment. The concentration of the standard is measured by a gas chromatograph with flame ionization detector (GC-FID, Sichromat; Siemens, Karlsruhe, Germany) with a capillary column (Al_2O_3) porous layer open tubing (PLOT); Chrompack, Middelburg, the Netherlands). An exponential fit to the concentration decrease directly yields the dilution rate (Buxmann et al., 2012; Bleicher, 2012).

During the intercomparison experiments the WS had a base path of 2 m and an aperture of F/25, with a total light path of 288 m diagonally arranged through the chamber, whereas the CE-DOAS light path was horizontally arranged with a mirror distance of 1.33 m. In order to determine the absolute light path in the cavity, O_4 measurements were carried out, as described above. For that purpose an additional tube was mounted in between the resonator inside the smog chamber. The maximal path length at 346.3 nm was 816 m. A sketch of the experiment setup is shown in Fig. 9. These experiments were described in detail by Buxmann (2012) and the results are described in Sect. 4.3.

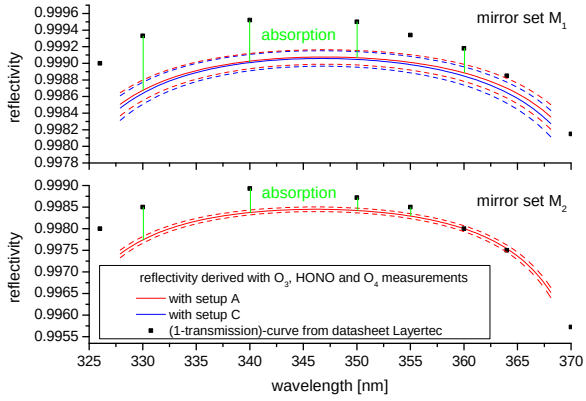

Fig. 3. Reflectivity curves of mirror sets M_1 and M_2: the black squares indicate the (1-transmission)-curve from the manufacturer's data sheet. The red and blue lines are the reflectivities calculated from measurements with setup A and C, respectively. The dashed lines are the accuracies of this determination, which are maximal 0.05 % within the second order polynomial fit range. The maximal reflectivities are $R_1 = 0.99910 \pm 0.00009$ for M_1 and $R_2 = 0.99840 \pm 0.00005$ for M_2 at 347 nm. The green lines between the black dots and the reflectivity curves indicate the losses due to absorption in the reflective layer. It can be seen that the absorption is small at 370 nm and increases towards shorter wavelengths.

4 Data evaluation and results

The software DOASIS (Kraus, 2004) was used for the analysis of the recorded spectra, as described in Sect. 3.1. The wavelength calibration of the spectrometer/detector was done with the help of the line spectra of a mercury lamp. For convolution of the literature absorption cross sections (overview in Table 3) with the instrument function, the recorded line shape at 334.14 nm of this lamp was used. For each trace gas a mean spectral shift was determined from a measured spectrum with strong absorption, and the cross sections were corrected with these mean shifts (Pre-shift, see Table 3) and linked together during the fit routine. For all trace gases the following DOAS fit settings were used: fit window 325–365 nm; high pass filter with 1000 iterations; 3rd degree polynomial; and spectral squeeze/stretch limited to ±2 % (of the total spectral range).

4.1 Mirror reflectivity and path length calibration

As described in Sect. 2.4, it is possible to use differential absorption structures to derive the wavelength dependence of the mirror reflectivity and therefore the determination of the wavelength-dependent path length.

We used O_3 and HONO to estimate the relative shape of the mirror reflectivity, not the absolute, as the actual concentrations of O_3 and HONO were unknown. The used fit windows are shown in Table 4. The relative shape was derived using a second-order polynomial fit, and the sensitivity of the O_3 and HONO measurements result in a maximum uncertainty of the relative shape of the reflectivity within the fitting range of 0.05 %. With the additional absorption bands of O_4 at 343.4 and 360.5 nm, the absolute reflectivity curve

Table 4. DOAS fit windows of O_3 and HONO for the determination of the relative wavelength-dependent path length.

Fit window	For HONO [nm]	For O_3 [nm]
1	325.5–337.2	326.5–329.8
2	337.3–349.1	329.5–332.7
3	348.7–359.0	332.7–335.8
4	361.4–375.6	335.8–339.2
5		338.9–342.7
6		342.4–346.6

of the mirrors could be determined with known concentration of O_4. The absolute reflectivity curves are shown in Fig. 3. The accuracy of the absolute reflectivity curves depends on the sensitivity of the HONO, O_3 and O_4 measurements. It is dominated by the sensitivity of the O_4 measurements, which is estimated according to Stutz and Platt (1996) to 2 %. Thus the total error of the absolute path length is estimated at 2 %. The following measurements were corrected with those reflectivity curves. The absorption A of the mirrors can be derived from the data in Fig. 3 as

$$A = (1 - T) - R. \tag{7}$$

The absorptions of both mirror sets are of the order of $A = 4 \times 10^{-4}$. According to Fiedler et al. (2007), the relation between optical light path length and signal-to-noise ratio Q can be determined with

$$Q = \frac{(1 - R - A)\left[1 + (1 - L)^2 R^2\right]}{\sqrt{\left[1 - (1 - L)^2 R^2\right]^3}}. \tag{8}$$

Figure 4 shows the enhancement factor (quality factor) Q dependency on $(1 - R)$ assuming $A = 4 \times 10^{-4}$. Based on this theory, we expected a lower detection limit for a reflectivity of $R_2 = 0.9984$ of M_2 than for M_1 ($R_1 = 0.9991$), if the measurement accuracy is purely dominated by photon noise.

4.2 Detection limits

The true 1σ error of the measurement of the different trace gases is obtained from the statistical 1σ error of the DOAS fit by multiplying with a factor of about 2.5 (depending on the ratio between width of the spectral features and the spectral resolution, etc.), as the fit error underestimates the true measurement error (Stutz and Platt, 1996), depending on the number of absorption bands, the number of channels used for evaluation, the intensity of the recorded spectrum, uncertainties in the wavelength-pixel mapping, and the scale and structures in the residual spectrum. The values are derived for measurements with relatively high trace gas concentration. Thus, measurement error and detection limit may actually be lower for lower concentrations due to weaker structures in the residual spectrum. The relative error decreases with

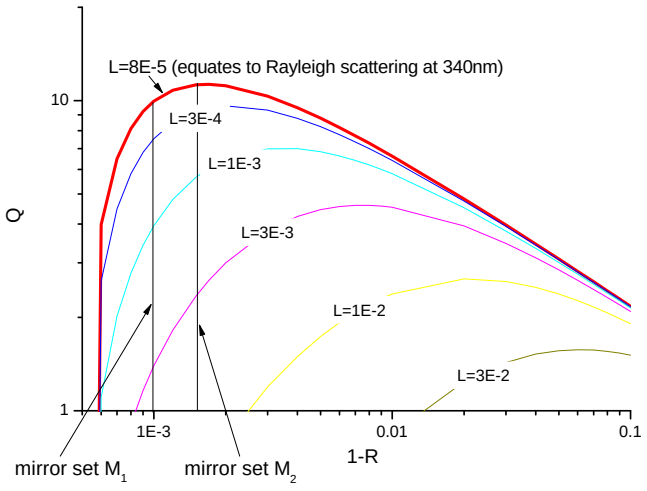

Fig. 4. Calculation of the enhancement factor (quality factor) Q from Eq. (8) (Fiedler et al., 2007) as a function of $(1 - R)$ for different losses L and a mirror absorption $A = 4 \times 10^{-4}$. The red line indicates the theoretical upper limit for Q for the minimal losses due to Rayleigh scattering in the resonator at 340 nm.

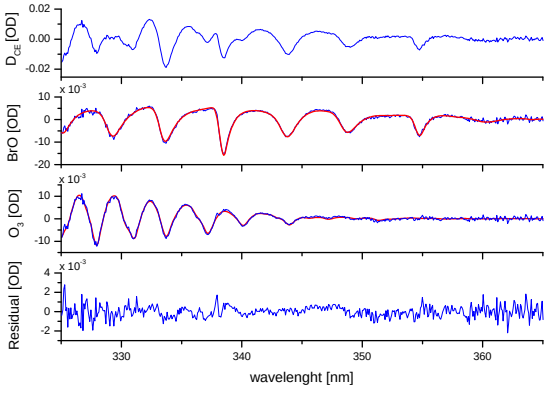

Fig. 5. Example of the spectral identification of BrO with the CE-DOAS setup. The thick red line indicates the fit result and the thin blue line the sum of the fit result and the residual. The corresponding mixing ratio for BrO is (507 ± 11) ppt and for O_3 (1984 ± 51) ppb. The residual is 4×10^{-3} peak to peak. Derived detection limits are based on measurements of gas mixtures (cf. Sect. 4.2).

higher concentrations. But at higher concentrations larger residual structures arise due to imperfect descriptions of the absorption bands. Thus, the absolute error and detection limit increase. The detection limit is given as twice the 1σ measurement error.

Example fits of different trace gases are shown in Figs. 5, 6, 7 and 8. The fit result in Fig. 5 shows an example where ozone and BrO were detected simultaneously, whereas only one absorber was present in the other examples (Figs. 6–8). Compared to the measurements where only individual

Table 5. Mean detection limits, including the presence of high ozone concentrations for different measurement configurations. Mirror set M_1 with $R_1 = 0.99910 \pm 0.00009$ and M_2 with $R_2 = 0.99840 \pm 0.00005$. The path length $\overline{L}_{\text{eff}}$ (at 347 nm) is for setup B = 839 m and for setup C = 1472 m, with an accuracy of 2 %. An estimate for the NO_2 detecion limit is given. Derived detection limits are based on measurements of gas mixtures (cf. Sect. 4.2).

Trace gas	Mirrors	Path length at 347 nm [m]	Integration time [min]	Det. lim. [ppt]	Integration time [min]	Det. lim. [ppt]
BrO	M_2	839	2.9	41	61.3	17
BrO	M_1	1472	4.8	20	80.8	11
HCHO	M_2	839	2.9	9100	61.3	5100
HONO	M_1	1472	4.8	970	106	450
O_3	M_1	1472	4.8	91 000	47.5	59 000
NO_2	M_2	816	2.9	3600		

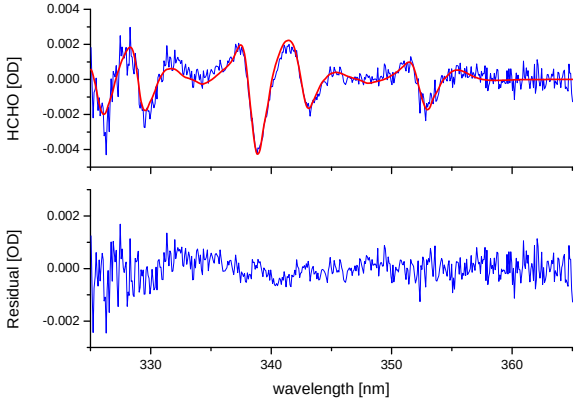

Fig. 6. Spectral DOAS fit of HCHO with (88 ± 6) ppb. Upper panel: the thick red line indicates the fit result and the thin blue line the sum of the fit result and the residual. Lower panel: fit residual with peak to peak 3×10^{-3}.

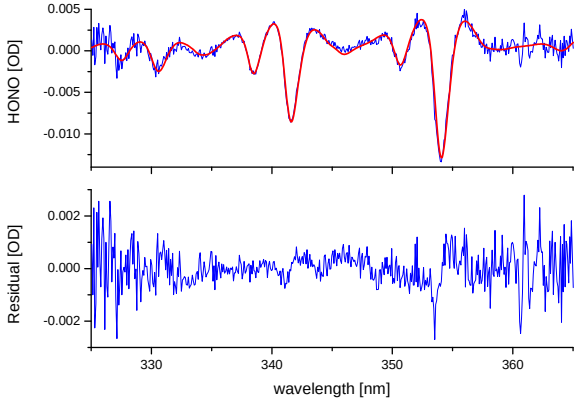

Fig. 7. Spectral DOAS fit of HONO with (16.0 ± 0.7) ppb. Upper panel: the thick red line indicates the fit result and the blue thin line the sum of the fit result and the residual. Lower panel: fit residual with peak to peak 4×10^{-3}.

absorbers were evaluated, the first example (Fig. 5) shows an approximately twice as large residual. This is typical for DOAS measurements. However, simultaneous detection and identification of the different absorbers is possible with sufficient sensitivity. The larger measurement error in these cases is considered in all data reported in this paper.

In Table 5 the detection limits for the measured trace gases for the two different mirror sets and different integration times are given. An estimated detection limit for NO_2 of 3.6 ppb at an integration time of 3 min is given as well. The differential NO_2 absorption (3×10^{-20} cm^2 molec^{-1}) in the wavelength range 325 nm–360 nm is relatively weak compared to BrO (3×10^{-17} cm^2 molec^{-1}), but concentrations could differ by 3 orders of magnitude in nature and thus be of the same magnitude. Nevertheless, other studies have also shown that NO_2 and BrO can be detected simultaneously and reliably by DOAS (Platt and Stutz, 2008; Mahajan et al., 2009; Pöhler et al., 2010).

Based on the theory of Fiedler et al. (2007), we expected a better detection limit for the lower reflectivity of $R_2 = 0.99840 \pm 0.00005$ for M_2 than for M_1 ($R_1 = 0.99910 \pm 0.00009$). However, we observed a better detection limit for M_1 compared to M_2. The reason is that in practice the detection limit of a DOAS measurement is not only dependent on the photon noise but also on spectral structures, which are not constant in time. Other sources increasing the noise are contributions from electronic noise and optical noise, e.g., additional noise introduced by the LED light source, optical fibers and spatial inhomogeneity of the optical grating of the spectrograph.

4.3 Instrument comparison

The BrO correlation plot (Fig. 10) shows very good agreement between the CE-DOAS and the WS-DOAS systems for mixing ratios from below the respective detection limits up

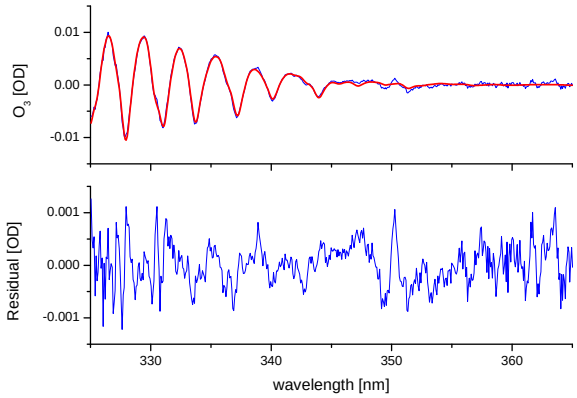

Fig. 8. Spectral DOAS fit of O_3 with (1766 ± 59) ppb. Upper panel: the thick red line indicates the fit result and the thin blue line the sum of the fit result and the residual. Lower panel: fit residual with peak to peak 2×10^{-3}.

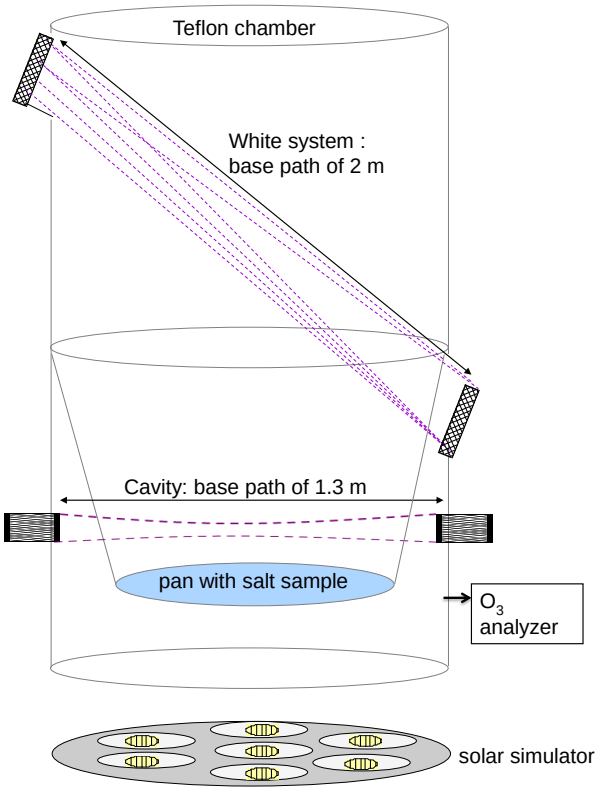

Fig. 9. Sketch of the multi-reflection cells used for DOAS in the Teflon chamber. A White system with a base path of 2 m was installed on a diagonal frame. The mirrors and prisms of the White system were mounted inside the chamber with additional Teflon bags. A maximum total light path of 320 m was achieved. The transfer optics adapts the opening aperture of the White system to the fiber and spectrograph. The CE-DOAS is mounted on a different frame, with a 1.3 m base path, resulting in an maximal light path of 816 m within these measurements (depending on the mirror reflectivity, here mirror set M_2 was used). The mirrors of the BrO cavity were constantly purged with clean air.

to 400 ppt. The slope of the BrO mixing ratios measured by each instrument is 1.06 ± 0.07, using a bivariate weighted fit as suggested by Cantrell (2008) to obtain a correlation coefficient of $r^2 = 0.95$. The agreement of HCHO of the two multi-reflection systems is remarkably good as well, with $r^2 = 0.998$ and a slope of 0.97 ± 0.03 for values up to 1 ppb, using again the bivariate fit (Fig. 11). The correlation plot for ozone furthermore shows (Fig. 12) a very good agreement between the CE-DOAS and the CL ozone monitor with a slope of 1.11 ± 0.08 and $r^2 = 0.92$, even though the CE-DOAS measurement spectral range was not optimized for ozone measurements. The excellent agreement between the two multi-reflection systems (WS and CE-DOAS), measuring at different light paths, demonstrates the accuracy and reliability of the newly developed CE-DOAS instrument. Integrity of operation is evident by the good agreement with the ozone monitor, which takes in air from a single location close to the chamber wall. This intercomparison of the instruments also demonstrates the rapid mixing of the chamber air within a timescale of 120 s (average time resolution of the instruments). A well mixed chamber is crucial for an understanding of the mechanistic of halogen release processes using chamber studies. A time series of a bromine explosion event with BrO mixing ratios of up to 360 ± 10 ppt is shown in Fig. 13. In the presence of high ozone mixing ratios of up to 350 ppb within the initial 30 min of the experiments, before the light was switched on, the BrO mixing ratio measured by the two DOAS instruments drops to slightly negative values (around -25 ppt on average). This negative offset is probably due to interference effects, which might not be captured by the DOAS evaluation, as well as an imperfect ozone literature reference spectrum. However, the values of BrO are not significant within the 2σ measurement error of 54 ppt. The heterogeneous formation of bromine caused a total ozone depletion of 320 ppb within 150 min. The very good detection limit of the CE-DOAS compared to the White system will allow performance of chamber studies close to natural BrO levels, which are typically in the range of several ppt up to more than 200 ppt (Saiz-Lopez and von Glasow, 2012).

5 Conclusions

We developed the first LED-based CE-DOAS for detection of BrO in the UV wavelength range from 325 to 365 nm. Due to the low power consumption of the light source, the instrument can be applied to field measurements with limited power supply. The achieved BrO detection limit is 11 ppt using a time resolution of 81 min per measurement. Besides

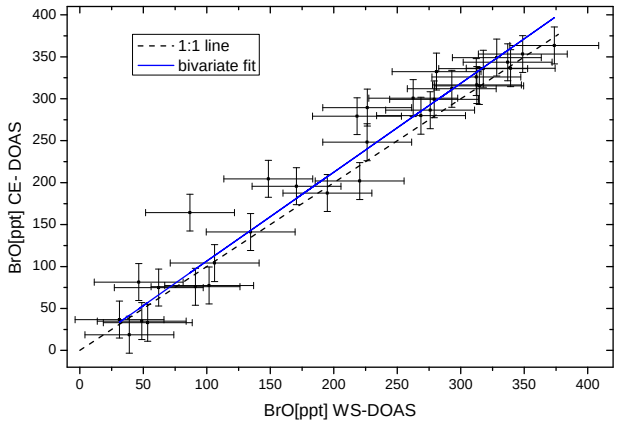

Fig. 10. Intercomparison of BrO detected by the White system and CE-DOAS simultaneously during a smog chamber experiment above a simulated salt pan, without injection of aerosols. The slope of the BrO mixing ratios measured by each instrument is 1.06 ± 0.07 using a bivariate weighted fit. The correlation coefficient is $r^2 = 0.95$.

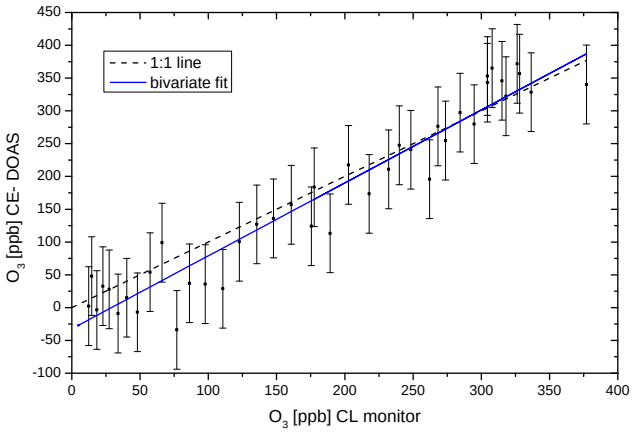

Fig. 12. Intercomparison of O_3 detected by the ozone monitor and CE-DOAS simultaneously during a smog chamber experiment above a simulated salt pan, without injection of aerosols. The slope of the O_3 mixing ratios measured by each instrument is 1.11 ± 0.08 using a bivariate weighted fit. The correlation coefficient is $r^2 = 0.92$.

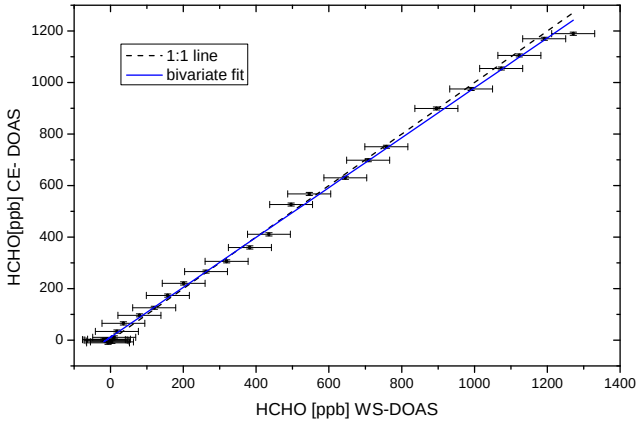

Fig. 11. Intercomparison of formaldehyde detected by the White system and CE-DOAS simultaneously during a smog chamber experiment above a simulated salt pan, without injection of aerosols. The slope of the HCHO mixing ratios measured by each instrument is 0.97 ± 0.03 using a bivariate weighted fit. The correlation coefficient is $r^2 = 0.998$.

BrO, also HONO, HCHO, O_3 as well as O_4 were detected in this wavelength range. The detection limits were 450 ppt for HONO, 5.1 ppb for HCHO, and 59 ppb for O_3. The advantage of the new UV LED CE-DOAS is that it is capable of measuring different species (e.g., BrO, O_3 and HONO) simultaneously and with little interference, although it is limited to areas with high concentrations and laboratory studies at the current state of development. Additionally the instrument measures the trace gases in comparison to most other in-situ instruments directly in the atmosphere minimizing losses or reactions on inlets, filters or walls. The detection limits are more than adequate for simulation chamber measurements, where BrO levels up to 6000 ppt were observed (Buxmann et al., 2012; Ofner et al., 2012). Additionally, the instrument can improve BrO measurements of chamber experiments due to its better accuracy than state-of-the-art DOAS White systems, which have BrO detection limits around 50 ppt for a time resolution of 4 min (Buxmann et al., 2012).

The relative dependence of the path length on the wavelength was determined using the absorption structures of O_3 and HONO. With an additional O_4 measurement at a known O_2 concentration, we calculated the absolute optical path length. Combining these data with the relative path length, the absolute wavelength-dependent mirror reflectivity and path length over the whole wavelength range was derived. We used two sets of mirrors with different maximal reflectivity values at 347 nm, M_1 with $R_1 = 0.99910 \pm 0.00009$ ($T = 0.05\,\%$) and M_2 with $R_2 = 0.99840 \pm 0.00005$ ($T = 0.12\,\%$). We determined the absorption for both mirror sets to be in the range of 4×10^{-4} at 347 nm. The absorption increases towards shorter wavelengths, so that the peak of the reflectivity is shifted towards larger wavelengths compared to the transmission of the mirrors.

In contrast to expectations based on the theory of Fiedler et al. (2007), we found a better detection limit for the higher reflectivity of M_1 than of M_2. The reason is that the detection limit of a DOAS measurement is not only dependent on the photon noise but also on spectral structures, which are not constant in time. Other sources for increasing noise are electronic noise and optical noise originating, e.g., from the LED

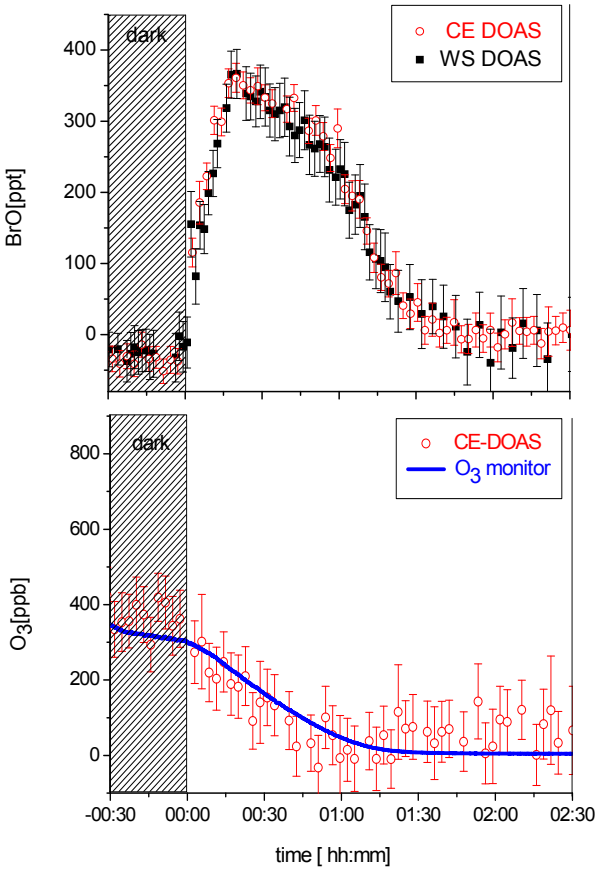

Fig. 13. Intercomparison of a time series of BrO (top panel) detected by the WS (black squares) and CE-DOAS (red open cycles) and O_3 (bottom panel) detected by the CE-DOAS (red open cycles) and O_3 monitor (blue line) simultaneously during a smog chamber experiment above a simulated salt pan. BrO is formed under irradiation (360 ppt within 17 min) and decreases to less than 30 ppt after 2 h. A corresponding total depletion of 320 ppb O_3 after 150 min is observed during the irradiation by the solar simulator.

light source, optical fibers and spatial inhomogeneity of the optical grating of the spectrograph.

Several options are possible for future improvement of the system: mirrors with higher reflectivity would lead to lower detection limits if the absorption of the mirrors could be reduced (e.g., by using different materials during the production process, which is currently under development by different companies). With the current absorptions, a higher reflectivity will not result in much lower detection limits. The base path length could also be expanded, but at the expense of compactness and ease of handling of the instrument setup. For most measurements this is not applicable.

Another aim is to increase the light intensity for a better time resolution and therefore improved detection limit. The intensity of UV LEDs is still very poor, but its improvement is a topic of current research at all LED manufacturers. Cooling of the LED also looks promising, since cooling of 30 K down to −10 °C was found to increase the radiation intensity up to 50 % (for an LED operation current of 1 mA), as expected from the data sheet (SET, 2010). While this work demonstrates that CE-DOAS measurements are feasible, applying UV LEDs as a light source, it is noted that xenon arc lamps may provide a 450-times higher input radiance. When compared to the electrical input, however, both devices deliver a similar radiance per input power. Therefore, UV LEDs may present a competitive alternative light source to xenon arc lamps, depending on the application of the respective instrument.

Furthermore, the system could be improved with a spectrometer with higher light throughput and larger entrance slit area to use more of the radiation exiting the cavity. Finally, we expect improvement of the detection limit from reduced optical noise. Our new UV LED CE-DOAS is a prototype instrument. Applying the above improvements and assuming that UV LED development will continue in the near future, we expect that accuracy and detection limit of the instrument can be improved by an order of magnitude during the next few years.

For validation an intercomparison between the CE-DOAS and a WS DOAS as well as between the CE-DOAS and a chemiluminescence (CL) ozone monitor was performed. Excellent agreement between the two multi-reflection systems (WS and CE-DOAS), measuring at different light paths and good agreement with the CL ozone monitor was achieved. This demonstrates the reliability of the newly designed CE-DOAS instrument.

Due to its compact size and low power consumption, it is possible to apply the BrO CE-DOAS instrument – besides in reaction chamber investigations – also in field studies with batteries even if other electrical power is not available. To our knowledge this instrument is the first mobile cavity-based BrO instrument in the UV wavelength range that is applicable to field measurements. Thus, in situ measurements with UV LEDs, especially of BrO, are possible in the future. As mentioned above, two other CE instruments exist for the detection of BrO (Chen and Venables, 2011; Grilli et al., 2012), but their field application seems to be limited due to size and power consumption.

Furthermore, BrO instruments with inlets, like CIMS (e.g., Liao et al., 2011) and mode-locked frequency-doubled CE spectrometer (Grilli et al., 2012) may suffer from the problem of inlet losses. Our novel UV LED CE-DOAS instrument provides a very good alternative, as it is an open path instrument without any inlets, and self-calibrating DOAS retrieval is used. We would like to stress that there are several areas where BrO has been detected in the atmosphere at levels exceeding the detection limit of the presented version of our CE-DOAS instrument, e.g., in arctic regions 41 ppt (Pöhler et al., 2010), at the Salar de Uyuni, Bolivia, up to 20 ppt (Hönninger et al., 2004), at the Dead Sea 200 ppt (Hebestreit et al., 1999; Matveev et al., 2001; Tas et al.,

2008), and in volcanic plumes where BrO mixing ratios of the order of 1000 ppt were inferred (Bobrowski et al., 2003). All these observations are averaged concentrations over few km-long light path lengths. Thus, the BrO CE-DOAS instrument could help to study the involved processes by deriving in situ BrO concentrations which are probably even higher. Moreover, it appears likely that the detection limits of our instrument will be greatly improved in the future.

Acknowledgements. We are grateful to the German Science Foundation (DFG) for funding the research unit 763, HALOPROC, to H.-U. Krüger (deceased) for technical support, to M. Sörgel for generation of HONO and to J. Ofner, S. Bleicher, and N. Balzer for helping with the chemical tasks.

Edited by: F. Stroh

References

Ball, S. M. and Jones, R. L.: Broad-Band Cavity Ring-Down Spectroscopy, Chem. Rev., 103, 5239–5262, 2003.

Ball, S. M., Povey, I. M., Norton, E. G., and Jones, R. L.: Broadband cavity ringdown spectroscopy of the NO_3 radical, Chem. Phys. Lett., 342, 113–120, 2001.

Ball, S. M., Langridge, J., and Jones, R.: Broadband cavity enhanced absorption spectroscopy using light emitting diodes, Chem. Phys. Lett., 398, 68–74, 2004.

Barrie, L. A., Bottenheim, J., Schnell, R., Crutzen, P., and Rasmussen, R.: Ozone destruction and photochemical reactions at polar sunrise in the lower Arctic atmosphere, Nature, 334, 138–141, 1988.

Barrie, L. A., Bottenheim, J. W., and Hart, W. R.: Polar Sunrise Experiment 1992 (PSE 1992): Preface, J. Geophys. Res., 99, 25313–25314, 1994.

Bleicher, S.: Halogenaktivierung im Aerosol und Salzpfannen -Experimente und Modellierung in einer Umweltkammer, Ph.D. thesis, Atmospheric Chemistry Research Laboratory, University of Bayreuth, Bayreuth, Germany, 2012.

Bobrowski, N., Hönninger, G., Galle, B., and Platt, U.: Detection of Bromine Monoxide in a Volcanic Plume, Nature, 423, 273–276, 2003.

Bottenheim, J. W., Gallant, A. C., and Brice, K.: Measurements of NO_y species and O_3 at 82° N latitude, Geophys. Res. Lett., 13, 113–116, 1986.

Bottenheim, J. W., Barrie, L. A., Atlas, E., Heidt, L. E., Niki, H., Rasmussen, R. A., and Shepson, P. B.: Depletion of lower tropospheric ozone during Arctic spring: The polar sunrise experiment 1988, J. Geophys. Res., 95, 18555–18568, 1990.

Buxmann, J.: "Bromine and Chlorine Explosion" in a simulated Atmosphere, Ph.D. thesis, Institute of Environmental Physics, University of Heidelberg, Heidelberg, Germany, 2012.

Buxmann, J., Balzer, N., Bleicher, S., Platt, U., and Zetzsch, C.: Observations of bromine explosions in smog chamber experiments above a model salt pan, Int. J. Chem. Kinet., 44, 312–326, doi:10.1002/kin.20714, 2012.

Buys, Z., Brough, N., Huey, L. G., Tanner, D. J., von Glasow, R., and Jones, A. E.: High temporal resolution Br_2, BrCl and BrO observations in coastal Antarctica, Atmos. Chem. Phys., 13, 1329–1343, doi:10.5194/acp-13-1329-2013, 2013.

Cantrell, C. A.: Technical Note: Review of methods for linear least-squares fitting of data and application to atmospheric chemistry problems, Atmos. Chem. Phys., 8, 5477–5487, doi:10.5194/acp-8-5477-2008, 2008.

Chen, J. and Venables, D. S.: A broadband optical cavity spectrometer for measuring weak near-ultraviolet absorption spectra of gases, Atmos. Meas. Tech., 4, 425–436, doi:10.5194/amt-4-425-2011, 2011.

Chen, J., Wenger, J., and Venables, D.: Near-ultraviolet absorption cross sections of nitrophenols and their potential influence on tropospheric oxidation capacity, J. Phys. Chem. A, 115, 12235–12242, doi:10.1021/jp206929r, 2011.

Engeln, R., Berden, G., Peeters, R., and Meijer, G.: Cavity enhanced absorption and cavity enhanced magnetic rotation spectroscopy, Rev. Sci. Instrum., 69, 3763–3769, 1998.

Fawcett, B. L., Parkes, A. M., Shallcross, D. E., and Orr-Ewing, A. J.: Trace detection of methane using continuous wave cavity ring-down spectroscopy at 1.65 µm, Phys. Chem. Chem. Phys., 4, 5960–5965, 2002.

Fiedler, S., Hese, A., and Ruth, A. A.: Incoherent broad-band cavity-enhanced absorption spectroscopy, Chem. Phys. Lett., 371, 284–294, doi:10.1016/S0009-2614(03)00263-X, 2003.

Fiedler, S., Hese, A., and Heitmann, U.: Influence of the cavity parameters on the output intensity in incoherent broadband cavity-enhanced absorption spectroscopy, Rev. Sci. Instrum., 78, 073104, doi:10.1063/1.2752608, 2007.

Fleischmann, O. C. and Burrows, J.: New ultraviolet absorption cross-sections of BrO at atmospheric temperatures measured by time-windowing fourier transform spectroscopy, J. Photochem. Photobiol. A, 168, 117–132, 2004.

Friess, U., Sihler, H., Sander, R., Poehler, D., Yilmaz, S., and Platt, U.: The vertical distribution of BrO and aerosols in the Arctic: Measurements by active and passive differential optical absorption spectroscopy, J. Geophys. Res.-Atmos., 116, D00R04, doi:10.1029/2011JD015938, 2011.

Gherman, T., Venables, D. S., Vaughan, S., Orphal, J., and Ruth, A. A.: Incoherent broadband cavity-enhanced absorption spectroscopy in the near-ultraviolet: application to HONO and NO_2, Environ. Sci. Technol., 42, 820–895, 2008.

Greenblatt, G. D., Orlando, J. J., Burkholder, J. B., and Ravishankara, A. R.: Absorption measurements of oxygen between 330 and 1140 nm, J. Geophys. Res.-Atmos., 95, 18577–18582, 1990.

Grilli, R., Mejean, G., Kassi, S., Ventrillard, I., Abd-Alrahman, C., Fasci, E., and Romanini, D.: Trace measurement of BrO at the ppt level by a transportable mode-locked frequency-doubled cavity-enhanced spectrometer, Appl. Phy. B,, 107, 205–212, doi:10.1007/s00340-011-4812-9, 2012.

Hak, C., Pundt, I., Trick, S., Kern, C., Platt, U., Dommen, J., Ordóñez, C., Prévôt, A. S. H., Junkermann, W., Astorga-Lloréns, C., Larsen, B. R., Mellqvist, J., Strandberg, A., Yu, Y., Galle, B., Kleffmann, J., Lörzer, J. C., Braathen, G. O., and Volkamer, R.: Intercomparison of four different in-situ techniques for ambient formaldehyde measurements in urban air, Atmos. Chem. Phys., 5, 2881–2900, doi:10.5194/acp-5-2881-2005, 2005.

Hausmann, M. and Platt, U.: Spectroscopic measurement of bromine oxide and ozone in the high Arctic during Polar Sunrise Experiment 1992, J. Geophys. Res., 99, 25399–25413, 1994.

Hebestreit, K., Stutz, J., Rosen, D., Matveiv, V., Peleg, M., Luria, M., and Platt, U.: DOAS measurements of tropospheric bromine oxide in mid-latitudes, Science, 283, 55–57, 1999.

Hoch, D. J.: Resonator Verstärkte Differentielle Optische Absorptions Spektroskopie: Labormessungen von BrO, HCHO, HONO und O_3, Diploma thesis, Inst. for Environmental Physics (IUP), Atmosphere and Remote Sensing, Ruprecht-Karls-Universität Heidelberg, Heidelberg, Germany, 2010.

Hönninger, G., Bobrowski, N., Palenque, E., Torrez, R., and Platt, U.: Reactive bromine and sulfur emissions at Salar de Uyuni, Bolivia, Geophys. Res. Lett., 31, L04101, doi:10.1029/2003GL018818, 2004.

Horbanski, M.: A Compact Resonator Based Instrument for DOAS Measurements of Ambient Nitrogen Dioxide, Diploma thesis, Inst. for Environmental Physics – IUP, Atmosphere and Remote Sensing, University of Heidelberg, Heidelberg, Germany, 2010.

Horbanski, M., Pöhler, D., and Platt, U.: iCE-DOAS: A new iterative evaluation algorithm for compact and light weight resonator based DOAS instruments, in preparation, 2014.

Kahan, T. F., Washenfelder, R. A., Vaida, V., and Brown, S. S.: Cavity-enhanced measurements of hydrogen peroxide absorption cross sections from 353 to 410 nm, J. Phys. Chem. A, 116, 5941–5947, doi:10.1021/jp2104616, 2012.

Kern, C., Trick, S., Rippel, B., and Platt, U.: Applicability of light-emitting diodes as light sources for active DOAS measurements, Appl. Optics, 45, 2077–2088, 2006.

Kraus, S.: DOASIS: DOAS Intelligent Sytem, Software, copyright 2004 Stefan Kraus, Institute of Environmental Physics, University of Heidleberg, Germany, in cooperation with Hoffmann Messtechnik GmbH, 2004.

Kreher, K., Johnston, P. V., Wood, S. W., and Platt, U.: Ground-based measurements of tropospheric and stratospheric BrO at Arrival Heights, Antarctica, Geophys. Res. Lett., 24, 3021–3024, doi:10.1029/97GL02997, 1997.

Langridge, J. M., Ball, S. M., and Jones, R. L.: A compact broadband cavity enhanced absorption spectrometer for detection of atmospheric NO_2 using light emitting diodes, Analyst, 131, 916–922, 2006.

Langridge, J. M., Laurila, T., Watt, R. S., Jones, R. L., Kaminski, C. F., and Hult, J.: Cavity enhanced absorption spectroscopy of multiple trace gas species using a supercontinuum radiation source, Opt. Express, 16, 10178–10188, 2008.

Leser, H., Hönninger, G., and Platt, U.: MAX-DOAS measurements of BrO and NO_2 in the marine boundary layer, Geophys. Res. Lett., 30, 1537, doi:10.1029/2002GL015811, 2003.

Liao, J., Sihler, H., Huey, L. G., Neuman, J. A., Tanner, D. J., Friess, U., Platt, U., Flocke, F. M., Orlando, J. J., Shepson, P. B., Beine, H. J., Weinheimer, A. J., Sjostedt, S. J., Nowak, J. B., Knapp, D. J., Staebler, R. M., Zheng, W., Sander, R., Hall, S. R., and Ullmann, K.: A comparison of Arctic BrO measurments by chemical ionization mass spectrometry and long path-differential optical absorbtion spectroscopy, J. Geophys. Res., 116, D00R02, doi:10.1029/2010JD014788, 2011.

Liao, J., Huey, L. G., Tanner, D. J., Flocke, F. M., Orlando, J. J., Neuman, J. A., Nowak, J. B., Weinheimer, A. J., Hall, S. R., Smith, J. N., Fried, A., Staebler, R. M., Wang, Y., Koo, J.-H., Cantrell, C. A., Weibring, P., Walega, J., Knapp, D. J., Shepson, P. B., and Stephens, C. R.: Observations of inorganic bromine (HOBr, BrO, and Br_2) speciation at Barrow, Alaska, in spring 2009, J. Geophys. Res., 117, D00R16, doi:10.1029/2011JD016641, 2012.

Mahajan, A. S., Oetjen, H., Lee, J. D., Saiz-Lopez, A., McFiggans, G. B., Plane, J. M. C.: High bromine oxide concentrations in the semi-polluted boundary layer, Atmos. Environ., 43, 3811–3818, doi:10.1016/j.atmosenv.2009.05.033, 2009.

Mahajan, A. S., Plane, J. M. C., Oetjen, H., Mendes, L., Saunders, R. W., Saiz-Lopez, A., Jones, C. E., Carpenter, L. J., and McFiggans, G. B.: Measurement and modelling of tropospheric reactive halogen species over the tropical Atlantic Ocean, Atmos. Chem. Phys., 10, 4611–4624, doi:10.5194/acp-10-4611-2010, 2010.

Matveev, V., Peleg, M., Rosen, D., Tov-Alper, D. S., Hebestreit, K., Stutz, J., Platt, U., Blake, D., and Luria, M.: Bromine oxide – ozone interaction over the Dead Sea, J. Geophys. Res., 106, 10375–10387, 2001.

Meinen, J., Thieser, J., Platt, U., and Leisner, T.: Technical Note: Using a high finesse optical resonator to provide a long light path for differential optical absorption spectroscopy: CE-DOAS, Atmos. Chem. Phys., 10, 3901–3914, doi:10.5194/acp-10-3901-2010, 2010.

Meller, R. and Moortgat, G.: Temperature dependence of the absorption cross sections of formaldehyde between 223 and 323 K in the wavelength range 225–375 nm, J. Geophys. Res.-Atmos., 105, 7089–7101, 2000.

Neuman, J. A., Nowak, J. B., Huey, L. G., Burkholder, J. B., Dibb, J. E., Holloway, J. S., Liao, J., Peischl, J., Roberts, J. M., Ryerson, T. B., Scheuer, E., Stark, H., Stickel, R. E., Tanner, D. J., and Weinheimer, A.: Bromine measurements in ozone depleted air over the Arctic Ocean, Atmos. Chem. Phys., 10, 6503–6514, doi:10.5194/acp-10-6503-2010, 2010.

Ofner, J., Balzer, N., Buxmann, J., Grothe, H., Schmitt-Kopplin, Ph., Platt, U., and Zetzsch, C.: Halogenation processes of secondary organic aerosol and implications on halogen release mechanisms, Atmos. Chem. Phys., 12, 5787–5806, doi:10.5194/acp-12-5787-2012, 2012.

O'Keefe, A. and Deacon, D.: Cavity ring-down optical spectrometer for absorption measurements using pulsed laser sources, Rev. Sci. Instrum., 59, 2544–2551, doi:10.1063/1.1139895, 1988.

Orphal, J. and Ruth, A. A.: High-resolution Fourier-transform cavity-enhanced absorption spectroscopy in the near-infrared using an incoherent broad-band light source, Opt. Express, 16, 19232–19243, 2008.

OSRAM: XBO 75W/2 Product datasheet, available at: , last access: 7 May 2013.

Paldus, B. A., Harb, C. C., Spence, T. G., Zare, R. N., Gmachl, C., Capasso, F., Sivco, D. L., Baillargeon, J. N., Hutchinson, A. L., and Cho, A. Y.: Cavity ringdown spectroscopy using mid-infrared quantum-cascade lasers, Opt. Express, 25, 666–668, 2000.

Peeters, R., Berden, G., Apituley, A., and Meijer, G.: Open-path trace gas detection of ammonia based on cavity-enhanced absorption spectroscopy, Appl. Phys. B, 71, 231–236, 2000.

Pöhler, D., Vogel, L., Friess, U., and Platt, U.: Observation of halogen species in the Amundsen Gulf, Arctic, by active long-path differential optical absorption spectroscopy, P. Natl. Acad. Sci. USA, 107, 6582–6587, 2010.

Platt, U. and Lehrer, E.: Arctic Tropospheric Ozone Chemistry, ARCTOC, Final Report of the EU-Project No. EV5V-CT93-0318, Heidelberg, 1996.

Platt, U. and Stutz, J.: Differential Optical Absorption Spectroscopy: Principles and Applications, Physics of Earth and Space Environments, Springer-Verlag, Berlin, Heidelberg, 2008.

Platt, U., Meinen, J., Pöhler, D., and Leisner, T.: Broadband Cavity Enhanced Differential Optical Absorption Spectroscopy (CE-DOAS) – applicability and corrections, Atmos. Meas. Tech., 2, 713–723, doi:10.5194/amt-2-713-2009, 2009.

Read, K., Mahajan, A., Carpenter, L., Evans, M., Faria, B., Heard, D., Hopkins, J., Lee, J., Moller, S., Lewis, A., Mendes, L., McQuaid, J., Oetjen, H., Saiz-Lopez, A., Pilling, M., and Plane, J: Extensive halogen-mediated ozone destruction over the tropical Atlantic Ocean, Nature, 453, 1232–1235, doi:10.1038/nature07035, 2008.

Ritz, D., Hausmann, M., and Platt, U.: An improved open path multi-reflection cell for the measurement of NO_2 and NO_3, in: Optical Methods in Atmospheric Chemistry, edited by: Schiff, H. I. and Platt, U., Proc. SPIE, 1715, 200–211, doi:10.1117/12.140211, 1993.

Saiz-Lopez, A. and von Glasow, R.: Reactive halogen chemistry in the troposphere, Chem. Soc. Rev., 2012, 6448–6472, doi:10.1039/C2CS35208G, 2012.

Saiz-Lopez, A., Plane, J. M. C., and Shillito, J. A.: Bromine oxide in the mid-latitude marine boundary layer, Geophys. Res. Lett., 31, L03111, doi:10.1029/2003GL018956, 2004.

Saiz-Lopez, A., Mahajan, A. S., Salmon, R. A., Bauguitte, S. J.-B., Jones, A. E., Roscoe, H. K., and Plane, J. M. C.: Boundary layer halogens in coastal Antarctica, Science, 317, 348–352, doi:10.1126/science.1141408, 2007.

Schuster, G., Labazan, I., and Crowley, J. N.: A cavity ring down/cavity enhanced absorption device for measurement of ambient NO_3 and N_2O_5, Atmos. Meas. Tech., 2, 1–13, doi:10.5194/amt-2-1-2009, 2009.

SET: UVTOP Technical Data, available at: http://www.s-et.com (last access: 23 April 2012), 2010.

Siekmann, F.: Freisetzung von photolabilen und reaktiven Halogenverbindungen aus salzhaltigen Aerosolen unter simulierten und troposphärischen Reinluftbedingungen in einer Aerosol-Smogkammer, Ph.D. thesis, Atmospheric Chemistry Research Laboratory, University of Bayreuth, Bayreuth, Germany, 2008.

Sihler, H., Kern, C., Pöhler, D., and Platt, U.: Applying light-emitting diodes with narrowband emission features in differential spectroscopy, Opt. Lett., 34, 3716–3718, 2009.

Simpson, W. R.: Continuous wave cavity ring-down spectroscopy applied to in situ detection of dinitrogen pentoxide (N_2O_5), Rev. Sci. Instrum., 74, 3442–3452, 2003.

Sturges, W. T., Schnell, R. C., Landsberger, S., Oltmans, S. J., Harris, J. M., and Li, S.-M.: Chemical and meteorological influences on surface ozone destruction at Barrow, Alaska, during spring 1989, Atmos. Environ., 27A, 2851–2863, 1993.

Stutz, J. and Platt, U.: Numerical analysis and estimation of the statistical error of differential optical absorption spectroscopy measurements with least-squares methods, Appl. Opt., 35, 6041–6053, doi:10.1364/AO.35.006041, 1996.

Stutz, J., Kim, E., Platt, U., Bruno, P., Perrino, C., and Febo, A.: UV-visible absorption cross section of nitrous acid, J. Geophys. Res.-Atmos., 105, 14585–14592, 2000.

Taira, M. and Kanda, Y.: Continuous generation system for low-concentration gaseous nitrous acid, Anal. Chem., 62, 630–633, doi:10.1021/ac00205a018, 1990.

Tas, E., Peleg, M., Pedersen, D. U., Matveev, V., Biazar, A. P., and Luria, M.: Measurement-based modeling of bromine chemistry in the Dead Sea boundary layer – Part 2: The influence of NO_2 on bromine chemistry at mid-latitude areas, Atmos. Chem. Phys., 8, 4811–4821, doi:10.5194/acp-8-4811-2008, 2008.

Thalman, R. and Volkamer, R.: Inherent calibration of a blue LED-CE-DOAS instrument to measure iodine oxide, glyoxal, methyl glyoxal, nitrogen dioxide, water vapour and aerosol extinction in open cavity mode, Atmos. Meas. Tech., 3, 1797–1814, doi:10.5194/amt-3-1797-2010, 2010.

Tuckermann, M., Ackermann, R., Golz, C., Lorenzen Schmidt, H., Senne, T., Stutz, J., Trost, B., Unold, W., and Platt, U.: DOAS-observation of halogen radical-catalysed arctic boundary layer ozone destruction during the ARCTOC-campaigns 1995 and 1996 in Ny-Alesund, Spitsbergen, Tellus B, 49, 533–555, doi:10.1034/j.1600-0889.49.issue5.9.x, 1997.

Varma, R. M., Venables, D. S., Ruth, A. A., Heitmann, U., Schlosser, E., and Dixneuf, S.: Long optical cavities for open-path monitoring of atmospheric trace gases and aerosol extinction, Appl. Optics, 48, B159–B171, 2009.

Vaughan, S., Gherman, T., Ruth, A. A., and Orphal, J.: Incoherent broad-band cavity-enhanced absorption spectroscopy of the marine boundary layer species I-2, IO and OIO, Phys. Chem. Chem. Phys., 10, 4471–4477, 2008.

Venables, D., Gherman, T., Orphal, J., Wenger, J., and Ruth, A.: High sensitivity in situ monitoring of NO_3 in an atmospheric simulation chamber using incoherent broadband cavity-enhanced absorption spectroscopy, Environ. Sci. Technol., 40, 6758–6763, 2006.

Voigt, S., Orphal, J., Bogumil, K., and Burrows, J.: The temperature dependence (203–293 K) of the absorption cross sections of O_3 in the 230–850 nm region measured by Fourier-transform spectroscopy, J. Photochem. Photobiol. A, 143, 1–9, 2001.

Voigt, S., Orphal, J., and Burrows, J.: The temperature and pressure dependence of the absorption cross-sections of NO_2 in the 250–800 nm region measured by Fourier-transform spectroscopy, J. Photochem. Photobiol. A, 149, 1–7, 2002.

Volkamer, R.: Absorption von Sauerstoff im Herzberg I System und Anwendung auf Aromatenmessungen am EUropean PHOto REactor (EUPHORE), Diploma thesis, Institute of Environmental Physics, University of Heidelberg, Heidelberg, Germany, 1996.

Volkamer, R., Junkermann, W., Wirtz, K., and Platt, U.: Formation of formaldehyde, glyoxal and methylglyoxal from the toluene + OH reaction in the presence of NO_x, poster presented at EGS XXVII General Assembly, Nice, France, 2002.

Washenfelder, R. A., Langford, A. O., Fuchs, H., and Brown, S. S.: Measurement of glyoxal using an incoherent broadband cavity enhanced absorption spectrometer, Atmos. Chem. Phys., 8, 7779–7793, doi:10.5194/acp-8-7779-2008, 2008.

White, J. U.: Long Paths of Large Aperture, J. Opt. Soc. Am., 32, 285–288, 1942.

White, J. U.: Very long optical paths in air, J. Opt. Soc. Am., 66, 411–416, 1976.

Zalicki, P. and Zare, R.: Cavity ring-down spectroscopy for quantitative absorption measurements, J. Chem. Phys., 107, 2708–2717, 1995.